

Received May 4, 2020, accepted May 16, 2020, date of publication May 21, 2020, date of current version June 4, 2020.

Digital Object Identifier 10.1109/ACCESS.2020.2996506

In Vitro Study on Smart Stent for Autonomous Post-Endovascular Aneurysm Repair Surveillance

SAYEMUL ISLAM[®]¹, (Graduate Student Member, IEEE), XIAOLEI SONG², ERIC T. CHOI³, JUNGKWUN KIM⁴, HAIJUN LIU², AND ALBERT KIM[®]¹

¹Department of Electrical and Computer Engineering, Temple University, Philadelphia, PA 19122, USA

Corresponding author: Albert Kim (albertkim@temple.edu)

This work was supported by Temple University startup fund.

ABSTRACT Endovascular aneurysm repair (EVAR) is an established and reliable surgical treatment of abdominal aortic aneurysm (AAA), where a covered stent is implanted to prevent blood flow in the aneurysm sac. Although current EVAR is an effective technique, it requires long-term monitoring for the post-operative complications (e.g., endoleak, stent occlusion), which usually requires expensive radiologic imaging techniques such as ultrasonography, computed tomography (CT), or magnetic resonance imaging (MRI). In this paper, we present an accessible and continuous post-EVAR surveillance scheme by developing a smart stent that features ultrasonic powering, blood flow sensing, and integrated wireless electronics. As the body of the smart stent, a piezoelectric membrane with a custom pore architecture is utilized. The benefits of the embedded pore architectures include the expansion and contraction to comply with a minimally invasive procedure and enhanced ultrasonic powering and sensing capability. The smart stent is able to expand up to 112% in diameter when stretched due to the negative Poisson's ratio. The ultrasound generates 0.23 mW of electrical power, which can sufficiently operate a low power wireless electronics. A comprehensive operation of the smart stent is demonstrated in vitro. The integrated flow sensor can measure blood flow ranging between 30 mL/min to 980 mL/min with an average sensitivity of 0.11 mV/mL/min. The wireless electronics transmit and receive such blood flow rate data by modulating the carrier frequency from 81 to 88 MHz from 1 m away. The developed smart stent prototype is the first step towards minimizing post-EVAR complications by providing early and frequent access to diagnostic information to patients and physicians.

INDEX TERMS Piezoelectric transducers, biomedical telemetry, ultrasonic transducers, sensors, implantable biomedical devices, endovascular aneurysm repair, stent.

I. INTRODUCTION

Abdominal aortic aneurysm (AAA) is the most commonly diagnosed arterial aneurysm, accounting for over 10,000 deaths in the United States every year [1]. Aneurysm refers to an abnormal bulge on the wall of the aorta or artery associated with the gradual thinning of the vessel wall. The mortality of AAA can be over 80% if it ruptures. As a preventative treatment, a vascular surgeon places a covered stent-graft that is a self-expanding metal frame with woven polyester material at the aneurysm site via a minimally invasive procedure. The stent-graft redirects blood flow away from the aortic wall, and this procedure is called Endovascular Aneurysm Repair (EVAR). Since its first implementation

The associate editor coordinating the review of this manuscript and approving it for publication was Vishal Srivastava.

in patients in 1991 [2], EVAR has become an exceedingly common technique that can minimize surgical trauma, reduce the length of hospital stays, obviate the need for full-body anesthesia, and decrease overall mortality rate [3], [4].

Despite the advances in stent technology and procedural techniques, persistent post-EVAR complications, such as endoleak, are still remained. Endoleak is direct or collateral blood flow into the aneurysm sac [5]. Some types of endoleak are associated with aneurysm expansion and rupture. One study shows that post-EVAR complications occur in 16% - 30% of the cases, among which 19% - 24% of the patients require secondary intervention to treat endoleaks [5]. Thus, periodic monitoring, also called post-EVAR surveillance, is highly recommended [4], [6].

Currently, post-EVAR surveillance is done using imaging technology such as computed tomography (CT) or duplex

²Department of Mechanical Engineering, Temple University, Philadelphia, PA 19122, USA

³Department of Vascular and Endovascular Surgery, Lewis Katz School of Medicine, Temple University, Philadelphia, PA 19140, USA

⁴Department of Electrical and Computer Engineering, Kansas State University, Manhattan, KS 66506, USA



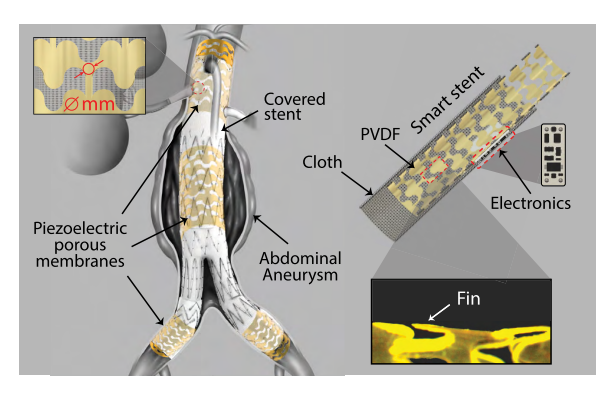


FIGURE 1. Example view of a smart stent that can monitor blood flow in the abdominal aneurysm.

ultrasound (DUS) [7]. Although these technologies can provide high-resolution images of the implanted stent-graft and surrounding tissues, they are expensive and require trained personnel. The patient follow-up is also challenging in an outpatient setting as the patients need to visit the clinic regularly to be scanned. It is reported that over 30% of patients were lost to follow-up after EVAR outside of clinical trials [8]. In addition, frequent imaging has a risk of nephrotoxicity due to the repetitive administrated iodinated contrast [9].

An alternative post-EVAR surveillance is direct pressure measurements within the aneurysm sac [10]–[12]. Although catheter-based pressure transducers have been used for this purpose [12], there are recent efforts to make the post-EVAR surveillance more frequent and continuous via wireless modality, allowing early detection of the complication and thereby further reducing the mortality. For example, an implantable MEMS pressure sensor (e.g., CardioMEMS) has been approved for clinical use [11]. The miniaturized pressure sensor is implanted within an aneurysm sac and provides pressure information. Another approach is a smart stent technology that integrates a MEMS pressure sensor on a stent body, which acts as a wireless antenna [13], [14]. For wireless interrogation, both technologies share the same technique. An integrated LC (i.e., inductor-capacitor) resonator in the implantable pressure sensor or smart stent is excited by an external electromagnetic field, which creates a reflected RF wave that contains pressure information. An external readout system then reads the pressure information wirelessly. Although it is a mature technology, challenges remain. In the human body, the wireless signal (i.e., electromagnetic field) is susceptible to higher tissue absorption and angular orientation. The long-distance between the stent system and the source coil can degrade the interrogation. The quality factor is usually low due to the small coil size [15]-[18]. Most importantly, the pressure information itself may not be sufficient to detect or predict the endoleak due to the complexity of the hemodynamics [6], [19], [20].

In this paper, we present a smart stent that could address the challenges of deep body energy delivery via ultrasonic powering, deep body communication via low-frequency RF signal, and seamlessly integrated blood flow sensing through flexible electronics (Fig. 1). The use of low frequency in

both ultrasonic powering and wireless communication allows deeper penetration due to the longer wavelength. Notably, ultrasonic powering is insensitive to the angular misalignment between a transmitter and a receiver (typical inductive powering requires a transmitter and a receiver to be placed in parallel) [15], [16]. The smart stent comprises multiple piezoelectric porous membranes deployed at multiple locations of a traditional covered stent (Fig. 1). These piezoelectric membranes act as ultrasonic power receivers as well as flow sensors. The location could be interior, exterior, proximal, mid, and distal. For example, we expect the piezoelectric membrane placed interior would detect the blood flow in circulation, whereas the piezoelectric membrane deployed exterior of a covered stent can detect the hemodynamics within an aneurysm sac. We experimentally demonstrate the piezoelectric membrane as a single ultrasonic receiver and a sensing element in vitro.

II. MATERIALS AND METHODS

The stent is based on a flexible piezoelectric polymer membrane (polyvinylidene fluoride, PVDF), which offers piezoelectricity, flexibility, biocompatibility, and easy fabrication [21], [22]. The membrane features a custom-designed perforation for two important functions: negative Poisson's ratio (NPR) and enhanced ultrasonic powering efficiency. The NPR due to the perforation allows the smart stent to expand transversely under an axial strain. The shape and pattern of the perforations can be optimized to enhance the ultrasonic response, i.e., the vibrational response to ultrasonic stimuli for both powering and sensing. A portion of the PVDF membrane is also utilized as a blood flow sensor, which generates an electrical voltage signal corresponding to the blood flow rate. The rest of the PVDF membrane converts incident ultrasonic waves into electric power to drive the integrated wireless electronics. As such, the overall design of the smart stent can be categorized into three main parts: 1) a piezoelectric PVDF membrane that is woven on a stent cloth as an ultrasound receiver, 2) a blood flow sensor that utilizes a portion of the PVDF membrane, and 3) integrated electronic circuits for power management, sensor readout, and wireless communication. Table 1 summarizes the design specifications of the smart stent.

The fabrication process is illustrated in Fig. 2. We start from a gold-plated PVDF thin film (Precision Acoustics U.K), which is cut into a smaller rectangular piece (30 mm × 62.8 mm, see Fig. 2(a)). These dimensions are determined based on the moderate-sized AAA. Note that the dimensions can be varied by the shape and location of the aneurysm. For example, the preoperative diameter of AAA can vary between 4 and 8 cm, depending on the patient, age, and location of the aneurysm [23]. Typically AAA interventions are required when diameter expands beyond 5.5cm [24]. However, for the demonstration purpose, the stent we built had a diameter of 2 cm and it showed full functionality at this dimension. When scaled to larger diameters, we expect the smart stent to receive more energy due to larger surface area

VOLUME 8, 2020 96341



TABLE 1. Summary of smart stent design specification.

PVDF membrane thickness	$110~\mu\mathrm{m}$
Density (ρ)	$1,780 \; { m kg/m^3}$
Piezoelectric constant (d_{33})	30 pC/N
Young's modulus (Y)	8.3 GPa
Bulk modulus (K)	4.3 GPa
Shear modulus (U)	3.5 GPa
Longitudinal velocity (c_L)	2,250 m/s
Shear velocity (c_S)	1,410 m/s
Relative dielectric constant (ϵ_r)	10 - 12
Poisson's ratio (ν_{pvdf})	0.18
Poisson's ratio $(\nu_{smart\ stent})$	-1.1
PCB dimension (length \times width)	$6~\mathrm{mm} \times 4~\mathrm{mm}$
PDMS layer thickness	$10~\mu\mathrm{m}$
Ultrasonic powering frequency	$14.0~\mathrm{MHz}$
Radio frequency range	81 - 87.74 MHz
Dimension (length \times diameter)	$30~\mathrm{mm} imes20~\mathrm{mm}$
Dimension of pore pattern	a = b = 1.3 mm
	c = 0.6 mm, d = 0.3 mm

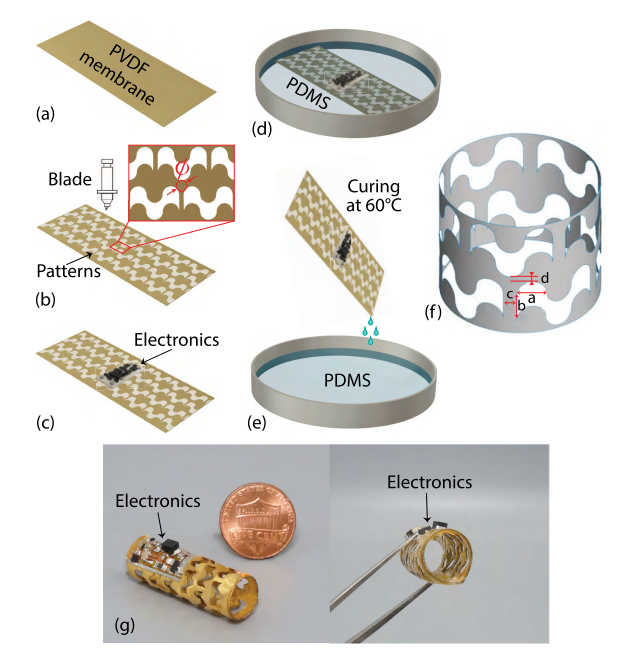


FIGURE 2. Device fabrication and integration: (a) plain PVDF film is cut into the desired shape, (b) patterns are cut on the solid film, (c) circuit fabrication, (d) PDMS passivation by submerging and (e) curing at 60°C, (f) dimension of patterns, (g) a fabricated smart stent with electronics.

interfacing with the incoming ultrasonic waves. After selecting the proper dimension, using a tungsten blade-equipped cutter plotter (Cameo 3, Silhouette Inc.), the PVDF film is patterned with a slightly modified re-entrant honeycomb (bow-tie) design with rounded corners (see Fig. 2(b)), which is inspired by the novel design with enhanced negative Poisson's ratio and Young's modulus reported by Lu et al. [25]. The modified bow-tie design also has a small fin-like structure acting as a flow sensor. The blood flow inside the stent will induce surface stress on the fin, resulting in voltage change due to piezoelectricity [26]. The flow sensors are then directly connected to the circuitry (the circuit design will be discussed later) (Fig. 2(c)). Note that we used three fins at the center of the PVDF thin film as flow sensors. The fins were electrically isolated from the body by laser ablating the gold surface on both sides of the thin film

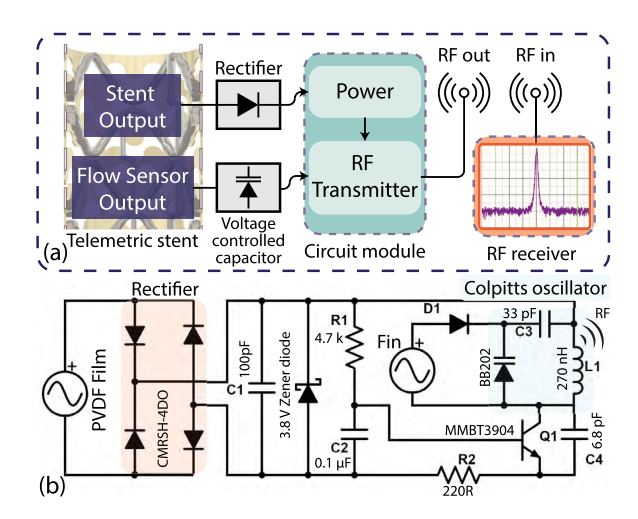


FIGURE 3. (a) System block diagram, (b) circuit diagram.

(Universal Laser System). The circuit was etched onto the PVDF surface using laser ablation, then surface mount electronic components were assembled using lead-free solder. The connection between the circuit with the PVDF membrane and sensors was bonded using conductive silver epoxy (8331, MG Chemicals) and the whole circuit was secured using a layer of UV curable glue to increase the mechanical strength and ensure reliability. The overall circuit dimension was $6 \text{ mm} \times 4 \text{ mm}$ for the prototype smart stent. Next, the perforated PVDF film with electronics is passivated by polydimethylsiloxane (PDMS). To create a thin layer (5 μ m on each side) of PDMS, the device is submerged in a pre-cured PDMS solution for 30 minutes (see Fig. 2(d)). Then it is taken out and fully cured in a vacuumed heater (60 °C) for another 30 minutes while hanged on a fixture (see Fig. 2 (e)). Lastly, the device is rolled and woven to a cylindrical shape, completing the smart stent (Fig. 2(f)). A prototype of a smart stent with an integrated circuit on the surface is shown in Fig. 2(g). Note that it can also be woven inside the cloth part of a stent in a similar manner a custom endograft stent is manufactured (i.e., weaving polyester clothe to the bare metal stent).

Fig. 3(a) illustrates a simplified block diagram, which consists of power management (i.e., an AC-to-DC rectifier) and a Colpitts oscillator-based RF transmitter circuit (i.e., FM transmitter). Fig. 3(b) shows a detailed integrated circuit design. A full-wave bridge rectifier using dual Schottky diodes (CMRSH-4DO, Central Semiconductor Corp., USA) with a 100 pF capacitor is assembled on the PVDF film surface. It converts the AC power induced by the incoming ultrasound (14-MHz continuous in our case) to DC power, which can drive the RF transmitter circuit. The RF transmitter processes the fin sensor output and transmits its information via a low-frequency RF signal. The fin sensor is connected to a voltage-controlled capacitor (BB202, NXP Semiconductors), which is a part of an LC tank of the Colpitts oscillator. The blood flow would induce correspondent voltage output from the fin sensor, resulting in frequency modulation of an RF transmitter. In our case, the capacitance in the LC tank is measured to be 12.2 - 14.3 pF.

96342 VOLUME 8, 2020



Pairing the variable capacitor with an inductor (L = 270 nH, B82422 × 100, TDK Corporation), we obtain the resonant frequency f_r by $f_r = 1/(2\pi\sqrt{LC})$, which is calculated to be in the range of 81 - 87.74 MHz. The RF signal is detected from outside of the body using a simple instrument such as a spectrum analyzer.

III. RESULTS AND DISCUSSIONS

To evaluate the smart stent, we performed three different sets of experiments. We characterized the mechanical expansion/contraction, ultrasonic powering, and flow rate *in vitro*.

A. MECHANICAL CHARACTERIZATION FOR ANGIOPLASTY PROCEDURE

conform with the minimally invasive procedure, we studied mechanical behavior using both simulation and experiment. The smart stent used in both simulation and experiment has a dimension of 30 mm × 20 mm (length × diameter). We defined the pattern arrangement by a center distance between the patterns, ϕ , as shown in Fig. 1 and Fig. 2(b). For simulation, we selected a smart stent with $\phi = 2.5$ mm, and the experiment used smart stent with $\phi = 2.5$, 3.5, and 4.5mm. We have experimentally measured the diameter expansion and fin angles from five samples for each ϕ group and measured three times per each sample. As indicated by the simulation data shown in Fig. 4(c), when the stent elongates, its diameter increases, confirming the stent has NPR (v = -1.1). The NPR is also experimentally validated. A custom-made fixture is used to hold and stretch the smart stent (Fig. 4(a)). During the stretch, time-sequence pictures (for example, Fig. 4(e) for $\phi = 2.5$ mm design) are taken using a digital camera (Sony, NEX-5N), from which we measure the diameter of the smart stent and the out-of-plane fin angles (Fig. 4(c) and 4(d)).

The maximum diameter that the smart stent achieves is 22.2 ± 0.4 mm (112% of the original size) (Fig. 4(c)). This expansion ratio can be enhanced by placing the unit cell of the NPR design more closely. It is expected that the smart stent with a closer unit cell ($\phi = 2.5$ mm) exhibits a 33% wider expansion compared to that with $\phi = 4.5$ mm. The results are consistent with the simulation results. Note that the PDMS encapsulation has negligible effects on the mechanical behavior of the smart stent. It is attributed to the rigidity of plate that is proportion to Eh^3 , where E is Young's modulus and h is the thickness. The PVDF has a thickness of 110 μ m and Young's modulus of 8.3 GPa. In comparison, the PDMS encapsulation layer is only 10 μ m, and Young's modulus is <1 MPa. These results indicate that the smart stent expands transversely under an axial strain, which can comply with a minimally invasive procedure. As it is also a thin film, it is expected to interface the clinical stent-graft easily. The prototype collapses structurally at some maximum diameter expansion, care must be taken to ensure the deformation is within the break-down limit.

To use the fin structures as flow sensors, we further investigate how the fins deform as the stent is stretched. It is

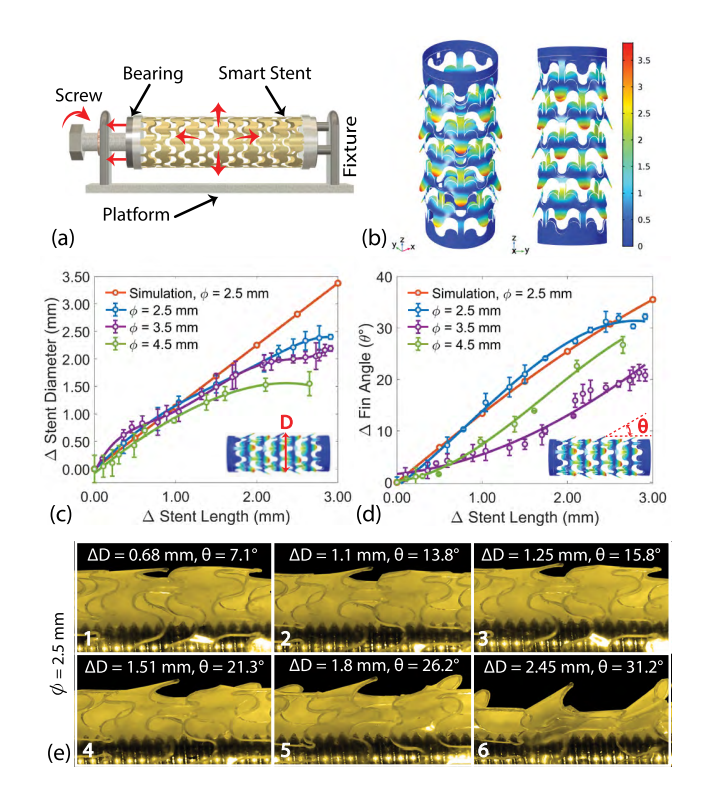


FIGURE 4. Mechanical test (a) experiment setup, (b) simulated expansion in COMSOL multiphysics, (c) diameter expansion, (d) increased fin angle during expansion, (e) time sequence picture of increasing fin angle.

observed that the fins gradually bend inward and outward in an alternating manner, while the smart stent is stretched. At the maximum diameter expansion (≈ 3 mm), the fin angle, denoted by the angular displacement θ in Fig. 4(d), is measured to be 34.8° and the maximum deployment amplitude for the fins was 0.5 mm. Thus, the fins bent inwards helps to detect the blood flow, whereas the fins bent outwards provides an anchor that holds the stent in place at the site of the aneurysm. Although the simulation and experimental results validate the expansion ratio due to design parameters, it did not include in vivo condition (e.g. immersion in the blood or fixation to the stent). The rigidity of the end conditions and pressure from the artery wall interferes with the mechanical responses, which may affect the ultrasound powering efficiency and blood flow sensing. However, the overall characteristics trend should be the same including the negative Poisson's ratio. It must be noted that the dynamic vibration response in the simulation has taken into account the surrounding watery medium, although it is also simulated under static and uniform conditions. As such, in our future research, the actual scenarios after implantation will be investigated both numerically and experimentally.

B. IN VITRO ULTRASONIC POWERING

After mechanical testing, the electrical performance, i.e., ultrasonic powering, is characterized. A water tank $(60 \times 30 \times 40 \text{ cm}^3)$ is used to mimic biological tissue as they have similar acoustic properties [27]. The experiment setup is shown in Fig. 5. An ultrasound transducer

VOLUME 8, 2020 96343

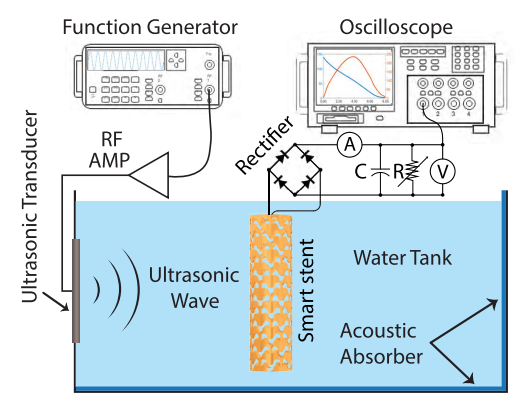


FIGURE 5. An experimental setup for electrical characterization.

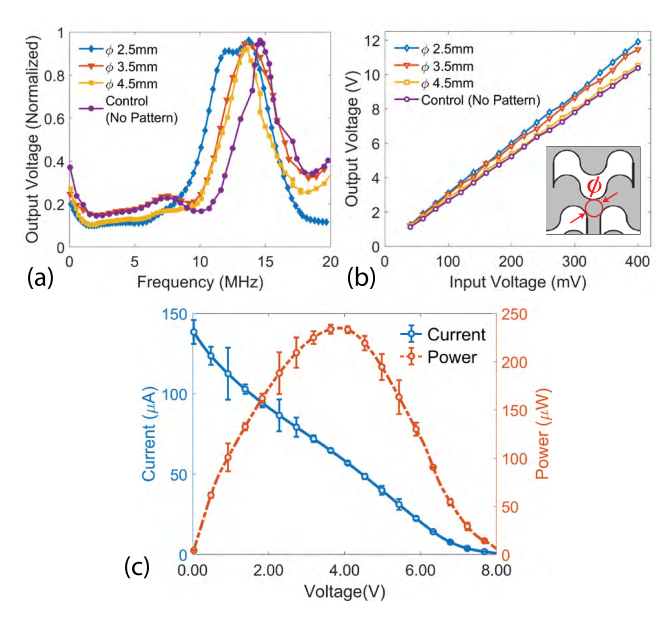


FIGURE 6. Electrical test: (a) frequency response, (b) voltage response, (c) I-V characteristics.

(lead zirconate titanate (PZT) transducer, $72 \times 72 \times 1$ mm³, Mide Technology, USA) is attached to one end of the water tank and driven by a continuous sinusoidal signal via a signal generator (4064, B&K Precision Corp.) connected to an RF amplifier (1040L, E&I Ltd.). This allows supplying ultrasonic waves to the smart stent. The receiver (smart stent) is positioned at 30 cm away from the transducer. The acoustic intensity is confirmed using a fiber optic hydrophone (FOHS64, Precision Acoustics, UK), which is controlled to be within the FDA limit of ultrasonic intensity for imaging applications (720 mW/cm²) [28].

First, the frequency is swept from 1 to 20 MHz to find the resonance frequency and the bandwidth of the smart stent. The output voltage from the smart stent is normalized by the acoustic intensity for the comparison. The peak voltage is observed near 14 MHz (resonance frequency) (Fig. 6(a)), which depends on the design parameter ϕ (see the inset of Fig. 6(b) and Fig. 2(b)): the more closely the patterns are placed, the lower the resonant frequency. It can be attributed to the overall compliance of the plate. As the pores are placed closer, a greater number of pores are placed in the

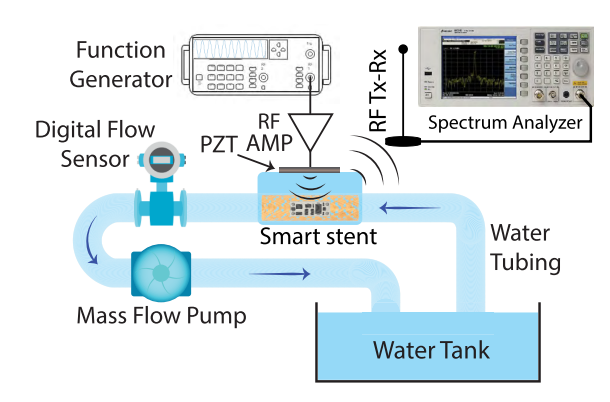


FIGURE 7. Experiment setup for sensor characterization.

given space, and thus the whole structure becomes more compliant.

The reduced plate rigidity also affects the overall vibration response. We observe a slightly higher voltage output from the smart stent with more closely placed patterns (Fig. 6(b)). The output voltage also depends on the input intensity. When the input voltage to the RF amplifier increases from 50 mV to 400 mV, the output open-circuit voltage of smart stent also increases linearly from 1.6 V to 12 V. There is a 13.2% improvement compared to the non-perforated control sample. This confirms that the higher vibrational response and thus the higher voltage output can be induced by adding perforations to the surface (Fig. 6(b)).

The power output is also investigated. In this experiment, the output is rectified and converted to DC voltage. Variable load resistance is connected across the storage capacitor. The current through the load resistance and the voltage across the load resistance (I = $60.5~\mu A$, V = 3.88~V) is adequate to power the RF transmitter circuit that sends the flow rate data to the external receiver. The calculated ultrasonic powering efficiency is 11.5%. The ultrasonic powering is able to generate up to the maximum short circuit current of $140~\mu A$. The optimal electrical power is measured to be 0.23~mW (UT transmitter consumed 2.05~mW when it is driven at 14~MHz).

It is noteworthy that all experiments were performed using a PDMS-encapsulated smart stent. Such passivation would be essential to protect the circuit in the aqueous environment and to ensure the safety from a short circuit of the PVDF membrane. As such, the resultant resonant frequency and voltage outputs accounted have taken the PDMS encapsulation into account.

C. IN VITRO WIRELESS COMMUNICATION CHARACTERIZATION

Finally, we conduct a comprehensive investigation of the smart stent using a closed-loop flow system (Fig. 7). A mass flow pump adjusts the water flow within a tubing while monitoring it by a digital flow meter (FS2012, Integrated Device Technology, Inc., USA). The smart stent is placed inside a larger diameter tubing, which mimics the fluidics flow in the aneurysm. The PZT transmitter is then placed on the tubing to transmit ultrasound to the smart stent. Because the blood flow is not a laminar flow but rather a turbulent and

96344 VOLUME 8, 2020



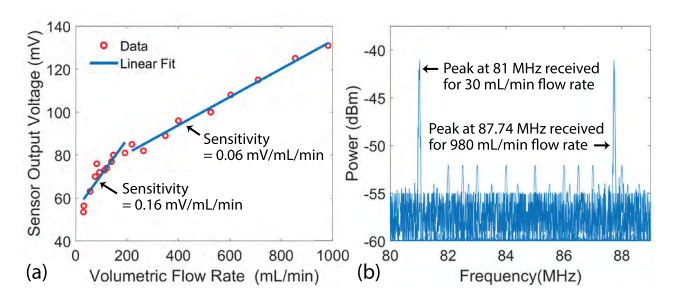


FIGURE 8. (a) Flow sensor voltage. (b) Spectrum analyzer output.

pulsed flow, the water pump is programmed to generate variable flow rates with the blood flow-like waveform. The smart stent then measures this change in flow rate using its fin and sends the RF signal to a dedicated receiver (i.e., a spectrum analyzer, N9320B, Keysight Technologies, Inc.).

The flow rate is controlled from 30 mL/min to 980 mL/min, which is based on a few clinical studies [29], [30]. The lower end of the blood flow is 30 mL/min, whereas the blood flow can reach up to 980 mL/min due to an occlusion in the artery. The corresponded sensor output is 53 mV – 131mV (Fig. 8(a)). In general, the output voltage increases linearly within the flow rates. Specifically, the sensor response has two linear regions: the first linear region is 30 - 200 mL/min with a sensitivity of 0.16 mV/mL/min, and the second linear region is 201 – 980 mL/min with a sensitivity of 0.06 mV/mL/min.

These voltage changes are detected by the shifts in the carrier frequency of the transmitted RF signal. A spectrum analyzer is placed approximately 1 m away from the experiment setup, i.e., the smart stent in a water tubing. For the given flow rate changes (30 - 980 mL/min), the frequency is varied between 81 – 87.74 MHz (Fig. 8(b)).

IV. CONCLUSION

In this paper, we demonstrate an ultrasonically powered smart stent with a flow sensing and wireless communication function. The smart stent can measure and send the blood flow information periodically whenever excited by ultrasound. Ultrasound, recognized as an FDA-approved technique, has superior advantages in transferring energy wirelessly to deeply implanted stent compared to inductive coupling due to less angular alignment sensitivity and lower tissue absorption. This method promises efficient power transfer to the electronics and increases interrogation distance. The integration of piezoelectric film eliminates the needs of a battery, which has been a significant bottleneck for the stent technology to integrate any electronics. The developed smart stent offers an alternative, portable, low-cost, and frequent monitoring for the post-EVAR surveillance in the out-patient setting. The smart stent can be further developed as a multimodal sensing platform to measure parameters such as pressure, flow rate, temperature, pH, and oxygen level. Overall, the developed smart stent can potentially provide convenient, early, and frequency access to critical diagnostic information, which can eventually minimize post-EVAR complications.

REFERENCES

- [1] E. J. Benjamin *et al.*, "Heart disease and stroke statistics—2018 update: A report from the American Heart Association," *Circulation*, vol. 137, no. 12, pp. e67–e492, 2018. [Online]. Available: https://www.ahajournals.org/doi/10.1161/CIR.00000000000000558
- [2] J. C. Parodi, J. C. Palmaz, and H. D. Barone, "Transfemoral intraluminal graft implantation for abdominal aortic aneurysms," *Ann. Vascular Surgery*, vol. 5, no. 6, pp. 491–499, Nov. 1991.
- [3] U. Blum, M. Langer, G. Spillner, C. Mialhe, F. Beyersdorf, C. Buitrago-Tellez, G. Voshage, C. Düber, V. Schlosser, and A. H. Cragg, "Abdominal aortic aneurysms: Preliminary technical and clinical results with transfemoral placement of endovascular self-expanding stent-grafts," *Radiology*, vol. 198, no. 1, pp. 25–31, 1996.
- [4] R. Greenhalgh, "Comparison of endovascular aneurysm repair with open repair in patients with abdominal aortic aneurysm (EVAR trial 1), 30-day operative mortality results: Randomized controlled trial," *Lancet*, vol. 364, no. 9437, pp. 843–848, 2004.
- [5] D. Daye and T. G. Walker, "Complications of endovascular aneurysm repair of the thoracic and abdominal aorta: Evaluation and management," *Cardiovascular Diagnosis Therapy*, vol. 8, no. S1, pp. S138–S156, Apr. 2018.
- [6] G. Maleux, M. Koolen, and S. Heye, "Complications after endovascular aneurysm repair," *Seminars Interventional Radiol.*, vol. 126, no. 1, pp. 3–9, 2009.
- [7] N. Pandey and H. Litt, "Surveillance imaging following endovascular aneurysm repair," Seminars Interventional Radiol., vol. 32, no. 3, pp. 239–248, Aug. 2015.
- [8] W. B. Jones, S. M. Taylor, C. A. Kalbaugh, C. S. Joels, D. W. Blackhurst, E. M. Langan, B. H. Gray, and J. R. Youkey, "Lost to follow-up: A potential under-appreciated limitation of endovascular aneurysm repair," *J. Vascular Surgery*, vol. 46, no. 3, pp. 434–440, Sep. 2007.
- [9] P. A. McCullough, "Contrast-induced acute kidney injury," J. Amer. College Cardiol., vol. 51, no. 15, pp. 1419–1428, Apr. 2008.
- [10] N. V. Dias, K. Ivancev, M. Malina, T. Resch, B. Lindblad, and B. Sonesson, "Intra-aneurysm sac pressure measurements after endovascular aneurysm repair: Differences between shrinking, unchanged, and expanding aneurysms with and without endoleaks," *J. Vascular Surg.*, vol. 39, no. 6, pp. 1229–1235, Jun. 2004.
- [11] H. Hoppe, J. A. Segall, T. K. Liem, G. J. Landry, and J. A. Kaufman, "Aortic aneurysm sac pressure measurements after endovascular repair using an implantable remote sensor: Initial experience and short-term follow-up," *Eur. Radiol.*, vol. 18, no. 5, pp. 957–965, May 2008.
- [12] P. G. Silveira, C. W. T. Miller, R. F. Mendes, and G. N. Galego, "Correlation between intrasac pressure measurements of a pressure sensor and an angiographic catheter during endovascular repair of abdominal aortic aneurysm," *Clinics*, vol. 63, no. 1, pp. 59–66, 2008.
- [13] X. Chen, B. Assadsangabi, Y. Hsiang, and K. Takahata, "Enabling angioplasty-ready 'smart' stents to detect in-stent restenosis and occlusion," Adv. Sci., vol. 5, no. 5, pp. 1–10, 2018.
- [14] B. John, C. Spink, M. Braunschweig, R. Ranjan, D. Schroeder, A. Koops, G. Woldt, I. Rauh, A. Leuzinger, G. Adam, and W. H. Krautschneider, "A stent graft occlusion detection: Pressure sensing implant device with inductive power and data telemetry," in *Proc. IEEE Int. Symp. Circuits Syst. (ISCAS)*, May 2018, pp. 4–7.
- [15] A. Denisov and E. Yeatman, "Ultrasonic vs. inductive power delivery for miniature biomedical implants," in *Proc. Int. Conf. Body Sensor Netw.* (BSN), Jun. 2010, pp. 84–89.
- [16] S. H. Song, A. Kim, and B. Ziaie, "Omnidirectional ultrasonic powering for millimeter-scale implantable devices," *IEEE Trans. Biomed. Eng.*, vol. 62, no. 11, pp. 2717–2723, Jun. 2015.
- [17] M. F. Mahmood, S. L. Mohammed, and S. K. Gharghan, "Ultrasound sensor-based wireless power transfer for low-power medical devices," *J. Low Power Electron. Appl.*, vol. 9, no. 3, p. 20, Jul. 2019.
- [18] H. Basaeri, D. B. Christensen, and S. Roundy, "A review of acoustic power transfer for bio-medical implants," *Smart Mater. Struct.*, vol. 25, no. 12, pp. 1–23, 2016.
- [19] K. Takahata, Y. B. Gianchandani, and K. D. Wise, "Micromachined antenna stents and cuffs for monitoring intraluminal pressure and flow," *J. Microelectromech. Syst.*, vol. 15, no. 5, pp. 1289–1298, Oct. 2006.
- [20] M. Allen, "Micromachined endovascularly-implantable wireless aneurysm pressure sensors: From concept to clinic," in 13th Int. Conf. Solid-State Sensors, Actuat. Microsyst. Dig. Tech. Papers (TRANSDUCERS), vol. 1, 2005, pp. 275–278.

VOLUME 8, 2020 96345



- [21] A. Vinogradov and F. Holloway, "Electro-mechanical properties of the piezoelectric polymer PVDF," *Ferroelectrics*, vol. 226, no. 1, pp. 169–181, Apr. 1999.
- [22] S. Islam and A. Kim, "Ultrasonic energy harvesting scheme for implantable active stent," in *Proc. IEEE Int. Microw. Biomed. Conf.* (IMBioC), Jun. 2018, pp. 70–72.
- [23] N. Peppelenbosch, J. Buth, P. L. Harris, C. van Marrewijk, and G. Fransen, "Diameter of abdominal aortic aneurysm and outcome of endovascular aneurysm repair: Does size matter? A report from EUROSTAR," J. Vascular Surg., vol. 39, no. 2, pp. 288–297, Feb. 2004.
- [24] S. Aggarwal, A. Qamar, V. Sharma, and A. Sharma, "Abdominal aortic aneurysm: A comprehensive review," *Exp. Clin. Cardiol.*, vol. 16, no. 1, pp. 11–15, 2011.
- [25] Z.-X. Lu, X. Li, Z.-Y. Yang, and F. Xie, "Novel structure with negative Poisson's ratio and enhanced Young's modulus," *Composite Struct.*, vol. 138, pp. 243–252, Mar. 2016.
- [26] Y. Xin, H. Sun, H. Tian, C. Guo, X. Li, S. Wang, and C. Wang, "The use of polyvinylidene fluoride (PVDF) films as sensors for vibration measurement: A brief review," *Ferroelectrics*, vol. 502, no. 1, pp. 28–42, Sep. 2016.
- [27] M. O. Culjat, D. Goldenberg, P. Tewari, and R. S. Singh, "A review of tissue substitutes for ultrasound imaging," *Ultrasound Med. Biol.*, vol. 36, no. 6, pp. 861–873, Jun. 2010.
- [28] Food and Drug Administration, "Marketing clearance of diagnostic ultrasound systems and transducers: Guidance for industry and food and drug administration staff," Food Drug Admin., Silver Spring, MD, USA, Tech. Rep. FDA-2017-D-5372, Jun. 2019.
- [29] D. N. Ku, "Blood flow in arteries," Annu. Rev. Fluid Mech., vol. 29, pp. 399–434, Jan. 1997.
- [30] P. Vaupel, F. Kallinowski, and P. Okunieff, "Blood flow, oxygen and nutrient supply, and metabolic microenvironment of human tumors: A review," *Cancer Res.*, vol. 49, no. 23, pp. 6449–6465, 1989. [Online]. Available: https://cancerres.aacrjournals.org/content/49/23/6449

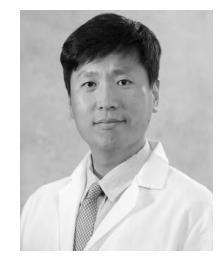


SAYEMUL ISLAM (Graduate Student Member, IEEE) received the B.Sc. degree in electrical and electronic engineering from the Ahsanullah University of Science and Technology, Dhaka, Bangladesh, and the M.Sc. degree in electrical engineering from Temple University, Philadelphia, PA, USA, where he is currently pursuing the Ph.D. degree with the Department of Electrical and Computer Engineering. He is also working with the Acousto-Micro Bioelectronics Labora-

tory (PI: Prof. Albert Kim), Temple University. His research interests include piezoelectric devices for powering and communication, wireless implantable microelectronic devices, and embedded systems.



XIAOLEI SONG received the B.S. degree from Zhengzhou University, Zhengzhou, China, and the Ph.D. degree in mechanical engineering in the field of machine tools and machining from the Beijing University of Technology, Beijing, China. He is currently pursuing the Ph.D. degree with the Dr. Haijun Liu's Group, Temple University. He is also working on acoustic sensors and acoustic metamatrials. His research is mainly about bio-inspired acoustic structures.



ERIC T. CHOI received the B.E.S. degree from Johns Hopkins University, in 1985, the M.D. degree from the University of Chicago, in 1990. He is a Research Fellowship in vascular surgery with Washington University, in 1994, and a Residency with Barnes Jewish Hospital, in 1999. His laboratory studies vascular smooth muscle cell (VSMC) dedifferentiation and anastomotic neointimal hyperplasia (NH) and its relevance to atherosclerosis and early arteriovenous fistula fail-

ure in metabolic disease. He is a Professor with the School of Medicine, Temple University. He is also the Chief of Vascular and Endovascular Surgery, the Chair of the Clinical Research Committee of CMDR, and a Professor of Surgery and Center for Metabolic Disease Research, Temple University.



JUNGKWUN KIM received the master's and Ph.D. degrees from the State University of New York at Buffalo, in 2007 and 2011, respectively. He was a Research Faculty with the University of Pennsylvania, from 2013 to 2016, and has two years of experience as a Postdoctoral Fellow with the Georgia Institute of Technology, from 2011 to 2013. He joined the Department of Electrical and Computer Engineering, Kansas State University, as an Assistant Professor, in 2016.



HAIJUN LIU received the Ph.D. degree in mechanical engineering from the University of Maryland, College Park (UMD), in 2012. He was a Postdoctoral Research Associate with the National Institute of Standards and Technology, Gaithersburg, MD, USA, and UMD. He is currently an Assistant Professor with the Department of Mechanical Engineering, Temple University. His area of expertise is in the fundamental science of sensor technology and its applications.

In particular, his researches focus on employing new sensing mechanisms inspired by nature, engineering advanced metamaterials, and developing a solid understanding of the pertinent mechanics. He was a Future Faculty Fellow at the A. James Clark School of Engineering of UMD, in 2009 and 2010.



ALBERT KIM received the B.S., M.S., and Ph.D. degrees in electrical and computer engineering from Purdue University, West Lafayette, IN, USA, in 2008, 2011, and 2015, respectively. He was a Research and Development Engineer with Intel Corporation, Hillsboro, OR, USA. He is currently an Assistant Professor with the Department of Electrical and Computer Engineering. He is also the Director of the Acousto Micro Bioelectronics Laboratory, Temple University. His research

is centered on biomedical applications of micro and nanotechnology. This includes a variety of devices and microsystems to address important clinical problems. He has collaborated closely with physicians in order to transfer the technology to the clinic.

• • •

96346 VOLUME 8, 2020